Catalysis Today xxx (xxxx) xxx

Contents lists available at ScienceDirect

Catalysis Today

journal homepage: www.elsevier.com/locate/cattod

Glucose dehydration reaction over metal halides supported on activated charcoal catalysts

Gabriel Delgado Martin [a], Beatriz Lara [a], Charf Eddine Bounoukta [a,b], María Isabel Domínguez [a], Fatima Ammari [b], Svetlana Ivanova [a], Miguel Ángel Centeno [a,*]

[a] Departamento de Química Inorgánica e Instituto de Ciencia de Materiales de Sevilla – Centro Mixto CSIC/Universidad de Sevilla, Avda. Américo Vespucio, 49, 41092 Sevilla, Spain

[b] Laboratoire de Génie des Procédés Chimiques, LGPC, Département de Génie des Procédés, Faculté de Technologie, Université FERHAT ABBAS SETIF-1, 19000 Setif, Algeria

ARTICLE INFO

Keywords:
Glucose dehydration
5-Hydroxymethyl furfural
Alkali
Alkali-earth
Activated charcoal

ABSTRACT

Different metal halide catalysts supported on a commercial active charcoal have been synthesized, activated, characterized and tested in glucose dehydration to 5-hydroxymethylfurfural using a biphasic water/methyl isobutyl ketone media. The influence of the cation nature (K^+, Ca^{2+}, Sr^{2+}, Mg^{2+}) and anion nature (F^-, Cl^-, Br^-) on the catalytic performance of the solid is discussed in terms of glucose conversion, HMF yield and products selectivity. The activation of the impregnated catalysts results in a great diversity of active sites, such as Bronsted sites (carboxylic groups), basic sites (metal oxide), and Lewis acid site (M^{n+}). Their distribution within the samples determinates the resulting products and the final HMF yield.

1. Introduction

The population growth and living standards improvements project for the near future a possible fossil fuel depletion. The later, together with the environmental awareness of the modern society, drives the recent investigations to look for renewable and sustainable alternatives for energy and industrial commodities production. Currently, there is a growing interest in the development of new technologies for renewable biomass conversion into energy vectors and chemicals as a way of substituting the non-renewable fossil feedstocks. Indeed, a large variety of chemical compounds that can be used directly as fuels or as platform molecules to produce valuable compounds, can be obtained from lignocellulosic biomass. This approach is known as biorefinery [1,2]. According to the US Department of Energy, one of the most interesting possibility is to transform the main carbohydrate monomer in biomass, glucose, into high value-added product 5-hydroxymethylfurfural (HMF) [3]. HMF is an organic compound containing furan ring with formyl and hydroxymethyl group in 2 and 5 positions respectively [1]. HMF is a compound of great versatility and multifunctionality, able to transform through biorefinery processes in a significant number of chemicals and biofuels [4,5] such as levulinic acid (LA), 2,5-dimethylfuran (DMF), 2, 5-bis(hydromethyl)furan (BHF), 2,5-diformylfuran (DFF), furan 2, 5-dicarboxylic acid (FDCA) or 2,5-furandimethanol (FDM), among others [1,5,6].

HMF can be produced from a variety of natural compounds. Cellulose would be the best candidate being a cheap and abundant polysaccharide, but its rigidity makes difficult its solubilization and causes important carbon loss and low yields to HMF [7–11]. Instead of cellulose the hexoses monomers (fructose or glucose) are preferred. Fructose transforms more efficiently and selectively in HMF but is not as abundant as glucose. Fortunately, fructose can be obtained easily by glucose isomerization. Thus, glucose converts in the best candidate due to its greater abundance, lower cost and high availability [10,12–14].

The glucose transformation to HMF takes place in a two-step reaction (Fig. 1). Firstly, glucose is isomerized to fructose (reaction catalyzed preferably by Lewis acid sites [11]) and the obtained fructose is dehydrated to HMF preferably on Brønsted acid sites[15], releasing three water molecules per fructose [16]. Some authors report the possibility of producing HMF from glucose via levoglucosan pathways [17–19]. Levoglucosan is obtained by glucose dehydration (one water molecule-loss process) with a subsequent second dehydration process to produce HMF with two more water molecules loss. It is also worth to mention the presence of secondary products such as formic (FA) and levulinic (LA) acid, obtained after HMF rehydration, and humins, produced by

* Corresponding author.
E-mail address: centeno@icmse.csic.es (M.Á. Centeno).

https://doi.org/10.1016/j.cattod.2023.01.019
Received 29 October 2022; Received in revised form 21 December 2022; Accepted 22 January 2023
Available online 23 January 2023

HMF-hexosespolymerization and/or condensation [20].

The use of water as a solvent is on the first place necessary, because of low glucose solubility in organic solvents, and environmentally friendly but favors the secondary reactions, such as HMF rehydration [11,21,22]. Nevertheless, the HMF selectivity can be improved by using biphasic water/organic system [23,24]. Since HMF is soluble in both, water and organic media, while the other reactants/products (glucose, fructose, levoglucosane, levulinic acid and FA) are only soluble in water, the utilization of a biphasic media can favor HMF partial extraction and protection against rehydration. Some studies indicate the use of aprotic organic solvents such as dimethyl sulfoxide (DMSO), dimethylformamide (DMF) or dimethylacetamide (DMA), as good candidates [25–29], but they have varied miscibility with water and high boiling points thus requiring high distillation temperatures at which the HMF become unstable. Ionic liquids can also be used as a solvents with melting temperatures below the boiling point of water and achieving high HMF selectivity [30–33], but their high price limits their use on a large scale [34].

In this work, methyl isobutyl ketone (MIBK) is chosen due to its chemical stability and low miscibility in water (19,2 g/L at 20ºC) [30], making it useful for further liquid-liquid extraction.

As for the catalyst, typically HCl or H_2SO_4 are used in homogeneous phase with important selectivity and activity. Nevertheless, their complex separation and recovery is rather costly and could lead to reactor corrosion problems. On the contrary, the heterogeneous catalysts are easy to recover and cause less environmental pollution [35,36]. Among the different heterogeneous catalysts described in the literature, H-form zeolites or transition metal phosphates can be found, although they lead to low selectivity and conversion to HMF [37]. On the contrary, active carbon-based catalysts are of particular interest due to their high chemical and mechanical stability, low price, inert nature, non-toxicity and great availability. Also, they can be modified by different agents or activation treatments, altering its textural, structural and chemical properties, allowing the optimization of the pore size and surface acidity and addition of different active sites [38–40]. Since the production of HMF requires acid centers, the use of carbonaceous materials makes even more sense taking into account the presence of surface oxygenated species, such as carboxylic groups, with Brønsted acidity [41]. These centers would act directly during the fructose dehydration to HMF reaction. However, the presence of Lewis acid centers is also needed in order to isomerize glucose to fructose. Thus, the combination of Brønsted and Lewis acid sites is necessary to successfully complete the conversion of glucose to HMF. In the literature, several examples of such type of tandem sites are reported [50–52] with the use of sulfonic groups [1], $ZnCl_2$ [42], HCl, $AgNO_3$ [43] or metallic halides [40]. The introduction of metal halides in the catalyst formulation is particularly interesting [24], since the metallic cation acts as Lewis acid center, favoring the isomerization to fructose, while the anion influences the yield and selectivity towards HMF formation [40].

For all above, in this work, different metal halide catalysts supported on a commercial active carbon are synthetized, characterized and tested in the glucose dehydration to HMF using biphasic water/MIBK media. The main objective is to study the influence of the nature of the cation (Ca^{2+}, Sr^{2+} or Mg^{2+}) and the nature of halide ion (F^-, Cl^- or Br^-) on the catalytic performances (glucose conversion and selectivity to the HMF and other side-reaction products).

2. Experimental

2.1. Materials

Darco® activated charcoal (*AC*), from Sigma Aldrich, potassium fluoride (KF) (Panreac) potassium chloride (KCl) (Normapur), potassium bromide (KBr) (Sigma-Aldrich), calcium chloride dihydrate ($CaCl_2{\cdot}2H_2O$) (Alfa Aesar), magnesium chloride hexahydrate ($MgCl_2{\cdot}6H_2O$) (Prolabo) and anhydrous strontium chloride ($SrCl_2$) (Alfa Aesar) were used for the synthesis of the catalysts.

For the catalytic reaction, D-glucose (Sigma-Aldrich) and methyl isobutyl ketone (MIBK) (Sigma-Aldrich) were employed.

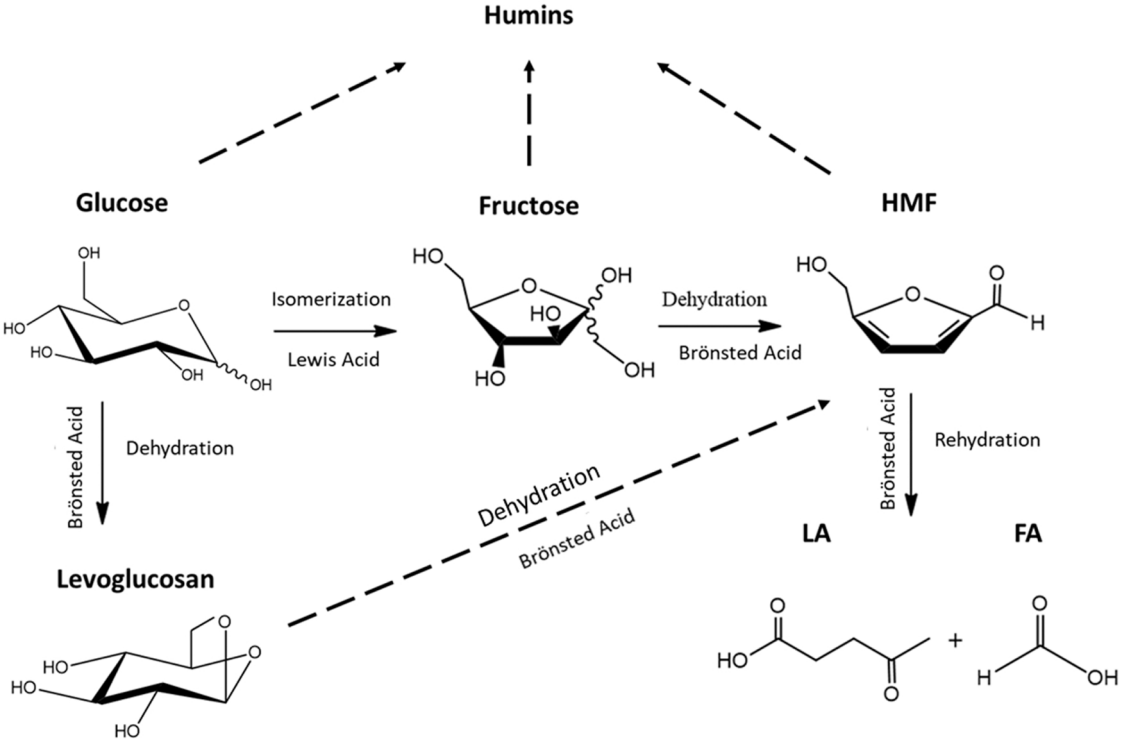

Fig. 1. Reaction scheme of glucose transformation to HMF.

2.2. Catalyst preparation

The solid catalysts were prepared by impregnating different metal halides ($CaCl_2$, $MgCl_2$, $SrCl_2$, KF, KCl and KBr) on the surface of a commercial activated carbon. In a typical preparation, 2 g of activated charcoal was added to a 40 mL aqueous solution of metal halide (1,6% molar) in a round bottom flask of 250 mL. The mixture was homogenized for 30 min in a rotary evaporator at 200 rpm and atmospheric pressure and room temperature. Subsequently, the solvent was evaporated at reduced pressure (72 mbar) at temperatures around 40 °C. The obtained solids were dried in an oven at 100 ºC for 24 h. The series of catalysts were labeled *MX/AC*, where *MX* is the used metal halide, and *AC* is the commercial charcoal. For example, *$MgCl_2$/AC* stands for magnesium chloride impregnated on activated charcoal.

2.3. Catalysts activation

The catalysts were activated by a heat treatment at 400ºC for 2 h with 10ºC/min heating ramp in the absence of oxygen using 100 mL/min of N_2, in a tubular quartz reactor allocated in horizontal furnace. This temperature is higher than that used in the catalytic tests, 180ºC, to stabilize the catalysts structure, avoiding as much as possible the catalyst evolution during reaction. After the activation process, samples were washed abundantly with warm water until the absence of chlorine ions was confirmed by $AgNO_3$ treatment. This procedure was applied to avoid the salt leaching and minimize the homogeneous contribution. The resulting catalysts were labeled *MX/AC act*. Thus, *$MgCl_2$/AC act* stands for magnesium chloride impregnated on activated charcoal and activated in the conditions described above.

2.4. Catalysts characterization

X-ray diffraction measurements were performed using Panalitycal X′Pert Pro diffractometer, with Cu anode (Cu-Kα 40 mA, 45 kV), with a step size of 0.05^0 and 300 s acquisition time within $10 - 90^0$ 2θ range. The phase determination of each diffraction pattern was performed by comparing it with the PDF2 ICDD2000 database (Powder Diffraction File 2, International Center f^{0}or Diffraction Data, year 2000).

The Scherrer equation was applied using the signals corresponding to the (002) and (100) carbon planes (Eqs. (1) and (2)) to estimate the size of the carbon crystallites:

$$L_c = \frac{K_c \lambda}{\beta_{002} \cos \theta_{002}} \quad (1)$$

$$L_a = \frac{K_a \lambda}{\beta_{100} \cos \theta_{100}} \quad (2)$$

where *Lc* is the crystallite height, *La* is the crystallite diameter, *K* is a shape factor depending on the crystal structure (*Kc* is 0.9 and *Ka* 1.84), λ is the wavelength of the X-radiation used (1.18 Å, Cu anode), β is the Full Width at Half Maximum (FWHM) and θ is the position of the peak maximum. The Scherrer equation was also used to determine the crystalline size of all other detected phases by XRD.

The textural properties were analyzed by N_2 adsorption-desorption measurements at 77 K with Micrometrics TRISTAR equipment. Before analysis, 100–200 mg of sample were outgassed under vacuum during 24 h, at 350 ºC in the case of activated samples and at 120 ºC in the case of non-activated ones. Specific surface areas were obtained by applying Brunauer-Emmett-Teller (BET) equation while the average sizes and distribution of pores were calculated from the desorption isotherm using Barrett-Joyner-Halenda (BJH) method.

Raman spectroscopy measurements were performed on a Horiba Jobin Yvon dispersive microscope (HR800) with confocal aperture of 1000 μm, a diffraction grating of 600 slots/mm and 50x objective. The equipment has a CCD detector, and a green laser ($\lambda = 532.05$ nm, maximum power 20 mW) was used working at 5 mW. In these conditions, the estimated laser spot diameter is 0.72 μm and the spatial resolution is 360 nm.

The amount of acid centers in the samples was determined by temperature programmed desorption of NH_3. 100 mg of sample were placed between quartz wools in a quartz reactor. After pretreatment with 50 mL/min of He flow at 200 ºC, samples were saturated with NH_3 at 100 ºC. Then, a 50 mL/min flow of He were introduced and, after 30 min of stabilization period (evacuation of the excess of NH_3), the temperature was raised up to 500 ºC with 10 ºC/min. NH_3 was followed by mass spectrometry on a Pfeiffer Vacuum Prisma Plus mass detector. For that, $m/z = 16$,17 and 18 signals were measured, and the ammonia evolution considered to be that of $m/z = 17$ minus the water contribution to this signal (26% of $m/z = 18$).

SEM images were taken on HITACHI S-4800 microscope equipped with secondary electron backscattered detector. The micrographs were taken at working distance of 15 mm and 20 kV voltage, at 100x and 1000x magnification. For the semi-quantitative compositional analysis, energy dispersive X-Ray spectroscopy (EDX) was used, operating at 15 mm working distance and 15 kV voltage. For composition mapping, the working distance was set to 15 mm, with voltage of 15 kV and 10,000x magnification.

2.5. Catalytic activity

The reaction of glucose to HMF dehydration was carried out in a 50 mL Schlenck reactor equipped with a Young valve at 180 ºC and magnetic stirring (600 rpm). 180 mg of glucose and 40 mg of the catalyst were introduced into the reactor containing 1.5 mL of water and 10.5 mL of MIBK. The reactor was closed and immersed in an oil bath at reaction temperature for 24 h. After that, the reaction mixture was cooled in an ice bath and filtered with a 0.45 μm nylon membrane. The organic and aqueous phases were analyzed by high performance liquid chromatography (HPLC Agilent 1260 series) equipped with a refractive index detector and a Hi-Plex H column (300 ×7.7 mm) using 0.01 M H_2SO_4 as mobile phase at 40 °C and 0.4 mL/min flow rate. One part of the aqueous phase was also analyzed with a Metacarb 87 ºC column, which separates better the hexoses and using MilliQ water as mobile phase at 75 ºC and a flow rate of 0.6 mL/min. The catalytic activity results were expressed in terms of glucose conversion, HMF yield and product selectivity as follows:

$$\text{Glucose conversion}(\%) = \frac{\text{moles of reacted glucose}}{\text{moles of initial glucose}} \times 100$$

$$\text{Product yield}(\%) = \frac{\text{moles of formed product}}{\text{moles of initial glucose}} \times 100$$

$$\text{Product selectivity}(\%) = \frac{\text{product yield}(\%)}{\text{glucose conversion}(\%)} \times 100$$

$$\text{Humins}(\%) = \left(1 - \frac{\text{final carbon moles}}{\text{initial carbon moles}}\right) \times 100$$

Humins direct detection was not possible due to their insolubility in the continuous phase, that is why it was considered as the detected carbon loss during the reaction.

3. Results and discussion

The commercial charcoal (*AC*) presents a typical diffraction pattern of amorphous carbon (Fig. 2) with signals at 2θ 23–25º, 42–44º and 80º. The first diffraction, assigned to the (002) plane family, arises from aromatic rings ordering and graphene sheets stacking through Van der Waals forces. The other two signals associated with the (100) and (110) planes, are ascribed to the in-plane desordered structure of the aromatic rings [44]. The commercial sample contains also silica in crystalline structural forms of cristobalite and quartz, with major diffractions at 2θ 22º and 27º, respectively. The narrow diffractions of silica overlap with

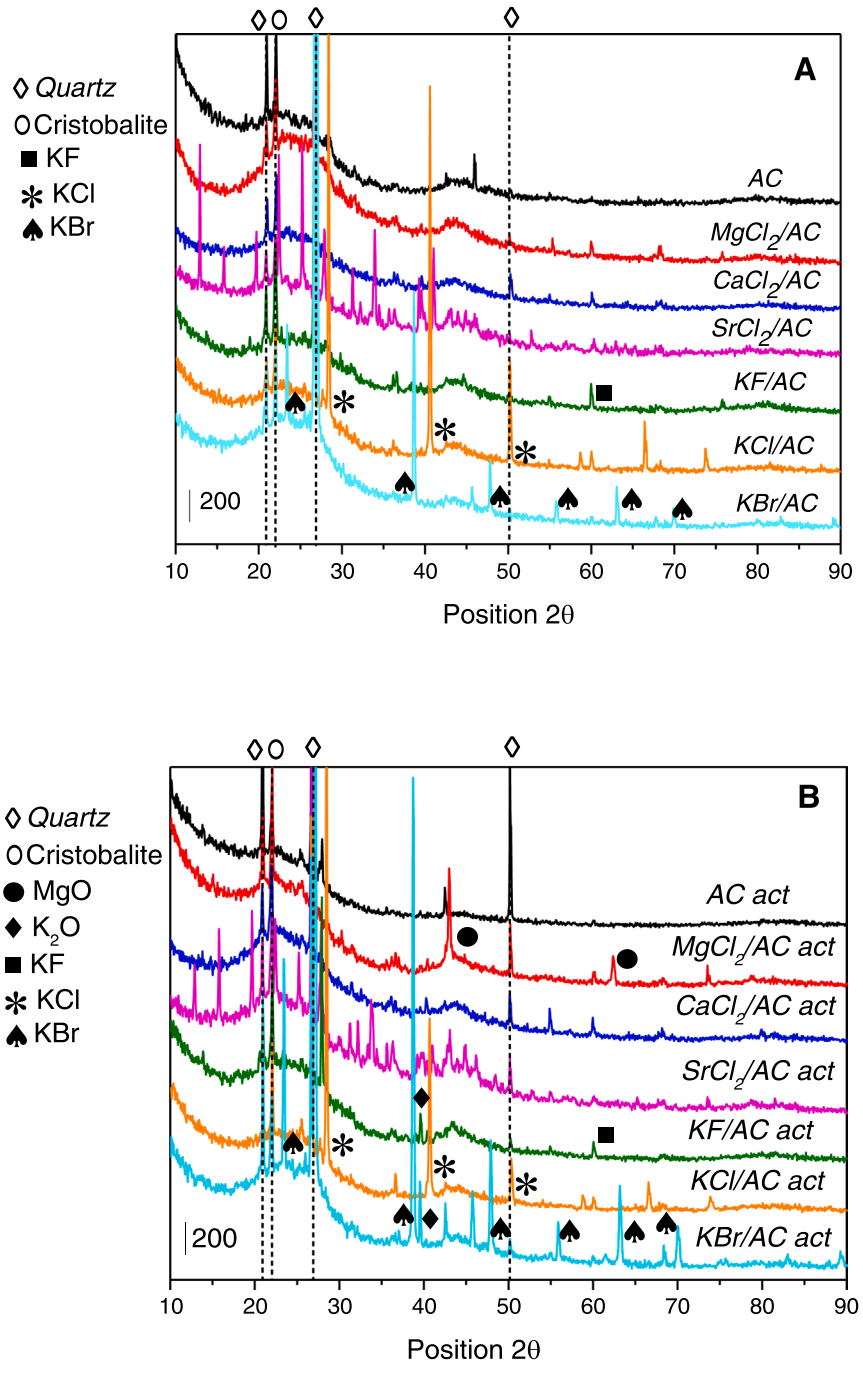

Fig. 2. Diffractograms of (A) fresh and (B) activated catalysts.

the broad diffraction of carbon. After impregnation the diffraction of the halides appears for all samples, exception made by $CaCl_2$/AC. The Lc and La values remain practically unaffected by the impregnation of halide and activation processes, although some changes in crystallite sizes are observed (Fig. 2 and Table 1).

The thermal activation of the catalysts, in addition to modifying the size of the crystals, leads in some cases to the detection/generation of new compounds from these halides (Fig. 2 and Table 1). While for the fresh *$MgCl_2$/AC* catalyst no diffractions corresponding to halide are observed, after activation both, the characteristic signals of $MgCl_2$ (JCPDS 00–037–0774) and MgO (JCPDS 01–077–2364) are visible. Something similar happens with *KF/AC* and *KF/AC act* samples. In *KF/AC act* sample the diffractions of halide (JCPDS 01–078–0657) are mixed with that of K_2O (JCPDS 00–023–0493) after the activation treatment. On the contrary, in the case of $CaCl_2$/AC sample, no diffractions associated neither to halide nor to oxide phase are visualized in both fresh and activated solids All detected phases are listed in Table 1.

For the rest of the samples, halides are observed in both the initial and activated samples. While in the samples with KCl (JCPDS 00–004–0587) no modification of the crystal size occurs, in the case of *KBr/AC* (JCPDS 01–072–1541) and *$SrCl_2$/AC* there is a modification of the crystal size with the activation. For the latter, the detected halide phases corresponds to hydrated chlorides with different degree of hydration: $SrCl_2{\cdot}(H_2O)_6$ (JCPDS 01–077–1375) and $SrCl_2{\cdot}(H_2O)_2$ (JCPDS 00–025–0891).

Fig. S1 represents the adsorption/desorption isotherms for the activated solids and their textural properties are summarized in Table 2. All isotherms are of type IV, according to the IUPAC classification [45,46],

Table 1
Lattice parameters of carbon and other crystalline phases detected.

	Crystallite lattice parameters			
	Carbon		Others	
Sample	*Lc* (nm)	*La* (nm)	Crystalline phase	Crystallite size (nm)
AC	1.5	2.9	SiO_2	
AC act	1.4	4.1	SiO_2	
$MgCl_2$/AC	1.3	4.1	–	–
$MgCl_2$/AC act	1.7	3.7	$MgCl_2$	89.0
			MgO	122.0
$CaCl_2$/AC	1.4	4.1	–	–
$CaCl_2$/AC act	1.4	5.0	–	–
$SrCl_2$/AC	1.3	3.7	$SrCl_2(H_2O)_2$	58.5
			$SrCl_2(H_2O)_6$	442.0
$SrCl_2$/AC act	1.4	3.6	$SrCl_2(H_2O)_2$	81.8
			$SrCl_2(H_2O)_6$	99.9
KF/AC	1.7	4.9	–	–
KF/AC act	1.4	5.1	KF	57.8
			K_2O	430.8
KCl/AC	1.4	3.6	KCl	372.5
KCl/AC act	1.7	3.7	KCl	372.5
KBr/AC	1.4	3.9	KBr	326.8
KBr/AC act	1.2	3.8	KBr	122.0

Table 2
Textural characteristics of activated samples.

Catalyst	BET Surface Area (m^2/g)	Microporosity (%)	BJH pore vol. (cm^3/g)	Pore diameter (nm)
AC	928	55.3	0.38	4.4
AC act	974	52.5	0.63	6.1
$MgCl_2$/AC act	875	52.1	0.56	6.1
$CaCl_2$/AC act	688	44.8	0.52	6.3
$SrCl_2$/AC act	723	49.1	0.50	6.3
KF/AC act	904	52.0	0.59	6.2
KCl/AC act	895	51.2	0.57	6.1
KBr/AC act	821	51.2	0.52	6.2

showing high amount of N_2 adsorbed at low relative pressures, indicative of a microporous material. Indeed, the calculated percentage of microporosity rounds 50% for all samples. All solids show H3-type hysteresis, typical of activated charcoals, and characteristic of particle' agglomerates forming pores of non-uniform size and/or shape. As for the BET surface area, it ranges from 688 m^2/g for *$CaCl_2$/AC act* to 904 m^2/g for *KF/AC act*, being in all cases lower than that of activated commercial charcoal (974 m^2/g). No major differences are observed in pore sizes and volumes within the series (Fig. S2 and Table 2). Although the software calculates an average pore size of 6 nm for all activated samples, the representation of the size distribution (Fig. S2) indicates a bimodal distribution, with major fraction of pores centered at 4 and 30–35 nm.

The textural properties of the commercial charcoal improved after the activation treatment (*AC* vs. *AC act*), reflecting in an increment in pores size, specific area and pores volume. Some variation in microporosity percentage is also evidenced, pointing out to a possible partial gasification of the carbon structure. This could be related to the decrease of the L_c parameter (Table 1) indicating also exfoliation process after thermal treatment. The presence of halide during activation drives to activated solids with lower textural properties, particularly lower BET surface areas (688 m^2/g to 904 m^2/g), due more probably to micropores blocking by the presence of other phase (halide or oxide). This can be also related with the observed increment in crystallinity deduced from XRD. No clear relation between textural properties and nature of the impregnated halide can be found. The lowest surface area observed for *$CaCl_2$/AC act* sample and the absence of diffractions ascribed to Ca-containing phases in XRD analysis could indicate simply that all calcium phases are well dispersed within the pores of the solid. It appears that the specific area increases with increasing the electronegativity of the halides within the K-containing series.

Fig. S3 shows a representative SEM micrograph for the activated carbon support, its general EDX spectrum and mapping corroborating the presence of silicon in the commercial sample. The micrographs, EDX spectra and mappings corresponding to the constituent elements, before and after activation are presented in Figs. S3 and S4. The morphology of the commercial charcoal remains unchanged after treatment no matter the metal halide used. For all samples the EDX analyses allow verifying the presence of the incorporated halides and metals. For the catalysts containing $MgCl_2$ or $CaCl_2$, the distribution of metal and halide is homogeneous over the whole analysed surface before and after activation. For all remaining catalysts, areas enriched in metal and the corresponding halogen are observed, indicating the presence of agglomerates or larger crystals in these samples, as evidenced by their crystallite size calculated in Table 2.

Table 3 shows the semi-quantitative compositional analysis of the different solids obtained from the EDX spectra. As expected, the main component is C and all samples show alkali or alkaline earth metal and corresponding halide. The obtained halide/metal ratios (X/M) are reasonably close to theoretical ones and considering that this is a semi-quantitative analysis. In the case of the $MgCl_2$ catalysts, a decrease in chlorine content is observed after activation reflecting its transformation to MgO [47,48], as revealed by XRD. *$SrCl_2$/AC* catalyst, also shows a lower X/M ratio for both, activated and un-activated solid. On the other hand, *KF/AC act* sample shows X/M ratio twice the theoretical one, due to the fact that the quantification of light elements such as fluorine implies a greater error.

As for the oxygen/carbon (O/C) ratio, it is observed that for the catalysts with alkali earth halides, this ratio is higher than that of the carbonaceous support. The contrary is true for the potassium halides series. Multiple reasons could explain that observation; i) the presence of metal oxide phases for the alkali earth halide series ii) higher degree of functionalisation of the catalyst surface or iii) heterogeneous distribution of SiO_2 impurities within the series. The activation process does not produce significant variation in the O/C ratio.

The fresh (a) and activated (b) samples show similar Raman spectra to that of commercial charcoal used as support (Fig. S5). The spectra are dominated by two main bands at 1340 and 1600 cm^{-1}, known as D- and G-band, respectively. The G-band is attributed to $E_{2\,g}$ symmetry vibration mode of the ideal graphite lattice and, therefore, is characteristic of the tension vibrations in the plane of C-C bonds with sp^2 hybridization. In the case of high crystallinity graphitic carbons, without defects, this band is the only visible during Raman analysis. The D-band on the contrary, is indicative of the presence of defects and imperfections, morphological, structural or compositional and corresponds to the $A_{1\,g}$ symmetry mode of vibration of graphite cell and the participation of carbon atoms with sp^3 hybridization [1]. The shape of the Raman spectrum in this region is complex and depends on the relative proportion of the different individual bands and is characteristic of the degree of crystallinity of the carbon. In our case, the Raman spectrum observed for all samples conforms to that of medium grade disordered (amorphous) carbonaceous materials [11,12,15,17,18,49–52]. The group of bands observed at higher Raman shifts (2680, 2940 and 3200 cm^{-1}) corresponds to the overtone bands (2D = 2680 cm^{-1} and 2 G = 3200 cm^{-1}) and combination (D + G = 2940 cm^{-1}) of these bands.

Apart from the bands due to C-C vibrations of the carbonaceous material, in some cases bands associated with quartz and cristobalite silica structures present in the starting commercial charcoal were also detected (Fig. S6) [53–55]. However, no bands assigned to metal halides are detected.

Table 3
EDX elemental analysis of the prepared samples.

Catalyst	C % atom	O % atom	X = Cl, F, Br %atom	M= Ca, K, Mg,Sr %atom	O/C ratio	X/M stoichiometric ratio	X/M ratio
AC	90.2	9.8			0.11		
AC act	88.6	11.4			0.13		
$MgCl_2$/AC	77.3	17.3	3.3	2.1	0.22	2	1.57
$MgCl_2$/AC act	82.8	15.0	0.3	1.8	0.18	2	0.17
$CaCl_2$/AC	77.1	16.3	4.4	2.2	0.21	2	2
$CaCl_2$/AC act	77.4	16.5	4.1	2.0	0.21	2	2.05
$SrCl_2$/AC	78.5	17.0	2.4	2.1	0.22	2	1.14
$SrCl_2$/AC act	80.7	14.5	2.9	1.9	0.18	2	1.53
KF/AC	89.3	5.6	3.0	2.1	0.06	1	1.43
KF/AC act	89.0	5.9	3.4	1.7	0.07	1	2
KCl/AC	88.8	6.8	2.4	1.9	0.08	1	1.26
KCl/AC act	90.9	6.1	1.4	1.5	0.07	1	0.93
KBr/AC	90.3	5.8	1.8	2.2	0.06	1	0.82
KBr/AC act	91.6	4.5	1.8	2.1	0.05	1	0.86

The ratio between the intensities of the G and D-bands (I_G/I_D) is usually used to estimate the degree of disorder and crystallinity, higher the ratio higher the crystallinity of the material (Table S1). The charcoals treated with metal halides have a higher I_G/I_D ratio than that of the starting carbon (*KCl/AC* the only exception) and these values are higher for the activated catalysts (Table 4) than for inactivated. This fact suggests that both, halide impregnation and subsequent thermal activation, lead to increase the order of the carbonaceous structure, in good agreement with the XRD data and increasing crystallinity (Table 1).

Fig. 3 shows the ammonia desorption profiles for all fresh and activated samples. Two type of NH_3 desorption signals can be observed, one at approximately 184 ºC and another at 284 ºC (330 ºC for *KF/AC act*), indicating the existence of two types of acid centers, weak (lower temperature) and medium-strong (higher temperature) [56]. In all cases, (activated or fresh samples) except for *KCl/AC act* and *KBr/AC act,* the centers of lower strength (desorption at 184 °C) are the main fraction. The NH_3 desorption temperature is lower for the non-activated catalysts (176ºC), which seems to indicate that the activation modifies, the strength of the acid sites. This supposition is confirmed also by the redistribution of the medium-strong and weak sites before and after the activation. It seems that a part of the weak sites presents for the fresh samples (unique desorption at lower temperature) transform to a medium-strong sites (appearance of the second desorption at around 280–300 °C for the activated samples).

Table 4 presents the ammonia desorption curve areas, which semi-quantitatively indicate the amount of acid centers capable of adsorbing NH_3 in solids. It can be seen that the number of acid centers of the starting carbon is practically zero. The addition of metal halides increases the amount of acid sites. In general, for the fresh samples the catalysts generated from potassium halides (KF, KBr and KCl) present smaller amount of acid centers than those prepared from Mg, Sr and Ca halides. For the last set of samples, the area under the desorption curve follows the sequence of the acidity of the cation (Mg^{2+}>Ca^{+2} > Sr^{+2}). The observed trend can be explained, taking into account the absolute hardness of the cations, higher the hardness higher the affinity to a hard base (NH_3) and higher the quantity of adsorbed ammonia.

After activation, the general difference between alkali and alkali earth halides is maintained but not the trend observed for the later.

Table 4
TPD-NH_3 adsorption areas of the prepared samples.

Catalyst	Area *m/z* (x10^4 a.u.)	Catalyst	Area *m/z* (x10^4 a.u.)
AC	0.44	***AC act***	0.04
$MgCl_2$/AC	32.10	***$MgCl_2$/AC act***	2.28
$CaCl_2$/AC	30.34	***$CaCl_2$/C act***	12.7
$SrCl_2$/AC	1.74	***$SrCl_2$/AC act***	4.06
KF/AC	0.00	***KF/AC act***	0.79
KCl/AC	0.00	***KCl/AC act***	2.16
KBr/AC	1.50	***KBr/AC act***	0.99

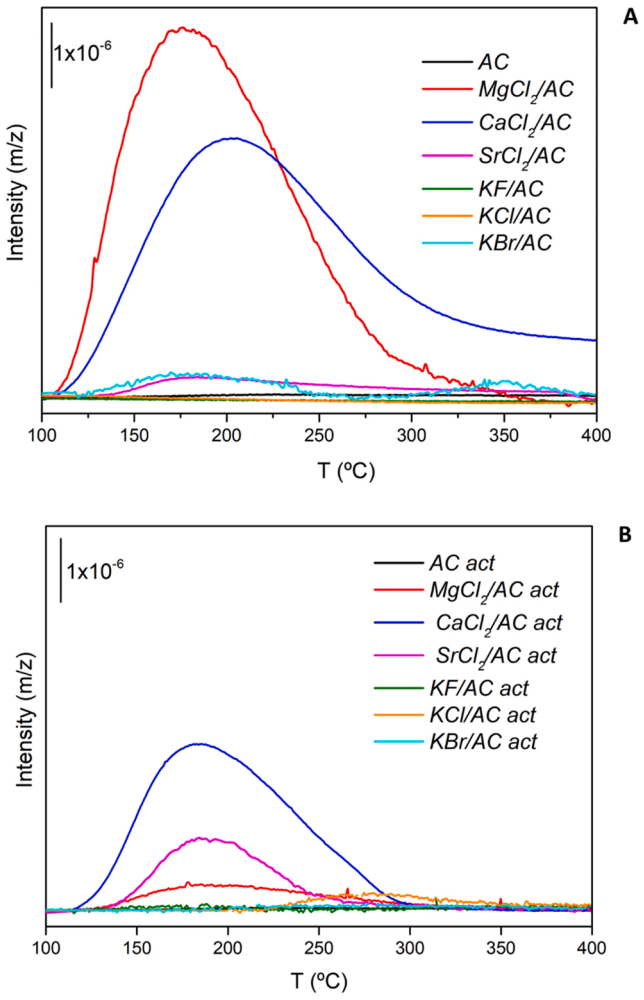

Fig. 3. NH_3 desorption profiles obtained by TPD of non-activated (A) and activated (B) catalysts.

$MgCl_2$/AC act and *$CaCl_2$/AC act* show fewer acid sites, possibly due to the formation of oxides basic in nature during the activation step. For all the other samples the amount of acid sites increases after activation.

3.1. Catalytic activity

The screening of the samples in glucose dehydration reaction at 180 °C in 24 h in terms of glucose conversion, HMF yield and products distribution is summarized in Fig. 4. The comparison between fresh (*AC*)

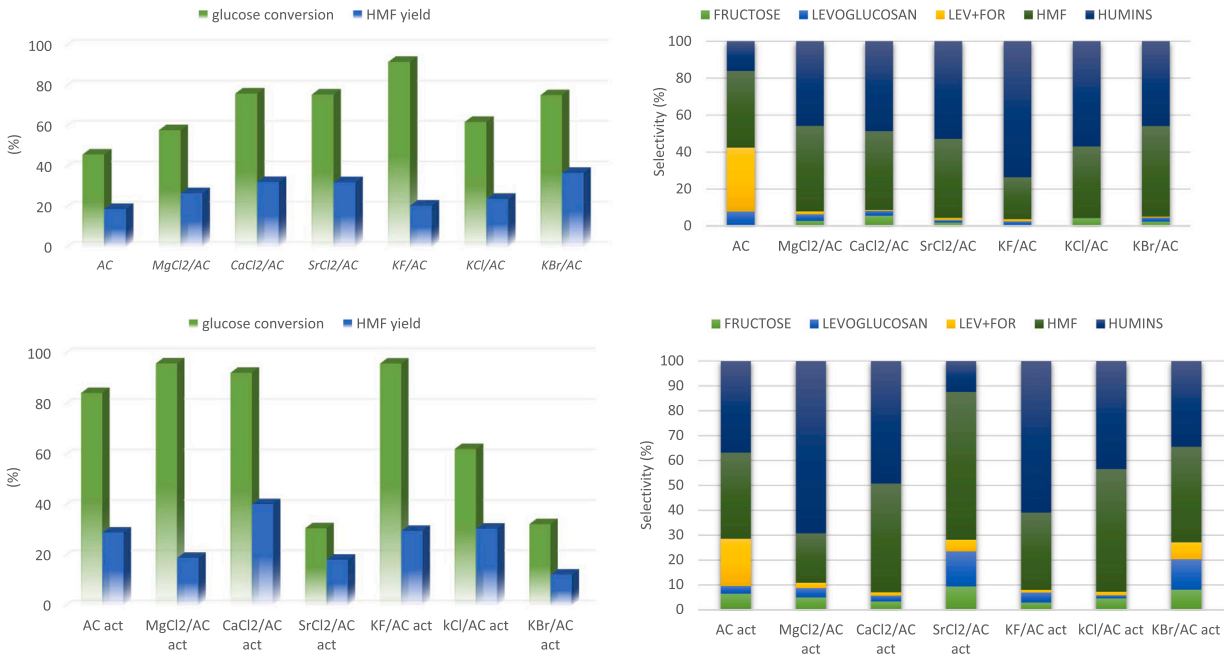

Fig. 4. Glucose conversion, HMF yield and products distribution over metal halide functionalized fresh (upper line) and activated (lower line) samples (Reaction conditions: T = 180 °C, time=24 h, MIBK/H_2O 7/1 V/V, $n_{glucose}$= 1 mmol, $m_{catalyst}$=40 mg).

and activated (*AC act*) charcoal allows us to evaluate the effect of the activation process and the washing procedure on the catalytic performance of the solid. Of course, in the case of non-activated samples, a partial solubilization of the active phase could occur, and consequently, the coexistence of homogenous and heterogeneous catalytic mechanisms is possible, as already reported in literature [57]. *AC act* presents a considerably higher glucose conversion (84 versus 46%) but the HMF yield does not reflect the same increase (29 versus 19% for *AC*) because of the selectivity decrease. In fact, the activation process leads to an increase in the humins selectivity (37 vs. 16% for *AC*) and a general increase of the humins/HMF ratio (1.06 vs 0.39 for *AC*). It is also significant that fructose is detected only for the *AC act* catalyst (6.5%) and levulinic and formic acids are more present for the fresh charcoal. The latter suggests that on the carbon surface different types of sites are present; mainly Brønsted sites for the fresh sample (carboxylic or other O-containing groups) that lost partially its character after activation (due to dehydroxylation). That is why, the Brønsted catalyzed products are more present for the fresh AC sample (levulinic and formic acid) and some Lewis acid or basic sites catalyzed products appears for the activated *AC act* sample (fructose).

While the glucose to fructose isomerization can be catalyzed either by Lewis acid sites or by the presence of any basic sites, the fructose to HMF dehydration and subsequent rehydration is preferred over Brønsted acid sites [16]. As revealed by TPD-NH_3, the activation process seems to involve a partial loss of carboxylic and acidic groups, generating basic sites. This could indicate a loss of Brønsted centers, which would explain the lower occurrence of the fructose to HMF dehydration reaction, leading to a lower selectivity to HMF and a generation of fructose.

Within the groups of impregnated carbons higher the glucose conversions, lower the HMF yields and higher the humins yields, suggesting a presence of an important number of active sites which not only converts glucose to HMF but also continue to catalyze its degradation to humins.

The change of cations for the chloride salts reflects in HMF yield increase in the following order $K^+ < Mg^{2+} < Ca^{2+} \approx Sr^{2+}$. The better performance of the alkali earth metals can be attributed to the formation of glucose – M^{2+} complexes able to immobilize the glucose structure and to catalyze its isomerization [58].

As for the effect of the anion, the HMF yield is observed to increase in the order $F^- < Cl^- < Br^-$, in good agreement with the results obtained by Wrigstedt et al. [40] using $CrCl_3 \cdot 6H_2O$ as co-catalyst and associated to an increase of fructose dehydration step rate.

After activation, no common trend is observed. While for the *$MgCl_2$/AC act*, *$SrCl_2$/AC act* and *KBr/AC act* catalysts the effect is negative (lower HMF yield but higher glucose conversion for *$MgCl_2$/AC act*), for the *$CaCl_2$/AC act* and *KF/AC act* catalysts there is a clear improvement in both parameters. In the case of the *KCl/AC act* catalyst, the conversion remains unchanged with activation but the HMF yield increases. The best catalyst by far is *$CaCl_2$/AC act*, with the highest yield of HMF (41%) and high glucose conversion (92%). The presence of bivalent cation, also Lewis acid (Ca^{2+}) and basic (CaO) sites could result in higher rate of glucose isomerization and high final yield of HMF.

Our results evidenced an important fact that higher glucose conversion implies lower selectivity to HMF. Likewise, higher glucose conversion is associated with higher humins production (Fig. 4), which is in agreement with one of the reported mechanisms for humins production via HMF- glucose cross-polymerization reactions [59]. In this sense, better quality criteria must be high selectivity to HMF and low humins production. Referring to this criterion, we could select *$SrCl_2$/AC act* as the most interesting catalysts (Fig. 5).

In order to study if the decrease of the reaction time would decrease the humins production, the reaction over the activated samples have been carried out in the same conditions but for 12 h (Fig. 6). The glucose conversion decreases for all samples and also decreases the humins production, especially for the chlorides containing samples (exception made by *$MgCl_2$/AC act*). It looks like for *$CaCl_2$/AC act* and *$SrCl_2$/AC act* samples attains an optimum, being almost all glucose converted into HMF. The presence of MgO for the *$MgCl_2$/AC act* catalyst (lower X/M and high O/C ratio for this sample), on the contrary, accelerates HMF and glucose conversion to humins, no matter the time of reaction indicating an important participation of the basic sites not only in the glucose to fructose isomerization but also in the cross polymerization. Another important fact is that *KF/AC act*, and *AC act* catalysts do not show any improvement in HMF selectivity at lower times indicating that low overall acidity (as seen by TPD-NH_3) results in low dehydration

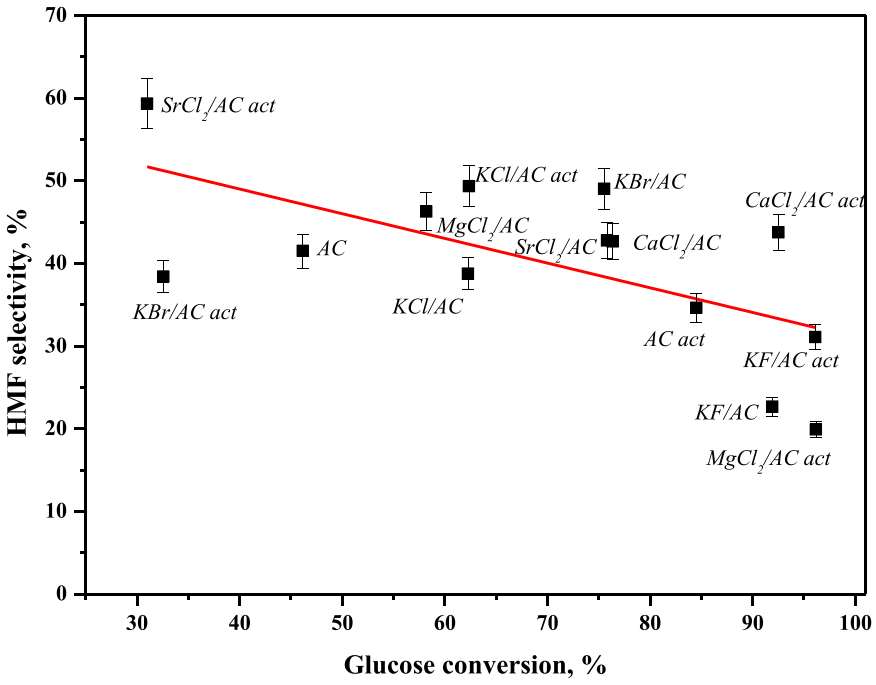

Fig. 5. Selectivity vs glucose conversion plot.

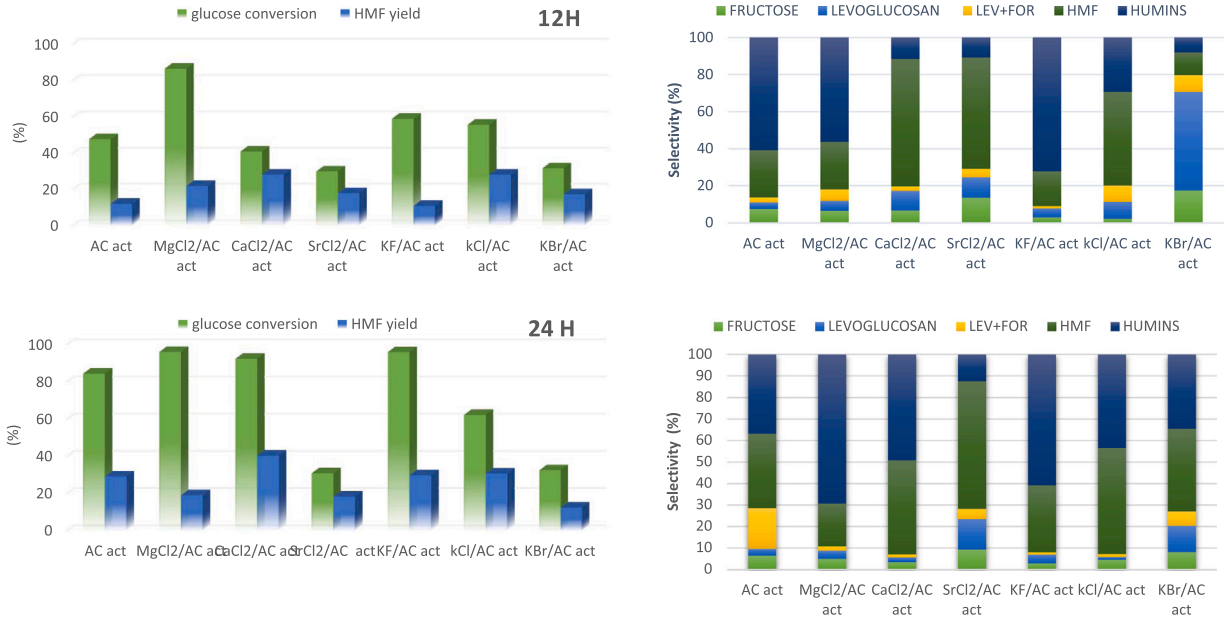

Fig. 6. Glucose conversion, HMF yield and products distribution over metal halide functionalized activated catalyst after 12 h of reaction (upper line) and 24 h of reaction (lower line) samples (Reaction conditions: T = 180 ºC, MIBK/H_2O 7/1 V/V, $n_{glucose}$= 1 mmol, $m_{catalyst}$=40 mg).

reaction rate.

Comparing only the HMF yields in both groups of experiments, the highest yields are obtained at 24 h of reaction although the *$CaCl_2$/AC act* catalyst working at 12 h is also very performant.

The reduction of time influences also the selectivity to fructose and levoglucosane indicating that the dehydration occurs through the mechanisms described above (via fructose or via levoglucosane) and that the nature of the anion is the one that influences the most the prevailing of one over another. It seems that Cl^- presence orient the reaction via fructose, while Br^- ions presence benefits levuglucosane formation (see selectivity of *KBr/AC act* sample).

3.2. Catalyst stability

To evaluate the recyclability and reusability of the systems four repetitive runs were performed over *$CaCl_2$/AC act* catalyst. The solid was separated by filtration and washed several times after each use and tested again in the next run under constant glucose/catalyst ratio. Fig. 7 shows glucose conversion and HMF yield after 12 h of reaction. The glucose conversion and yields of HMF remain similar in all runs, indicating a good stability and recyclability of the catalytic system. Moreover, these results also evidence that no significant leaching of active phase occurs during the reaction on activated samples.

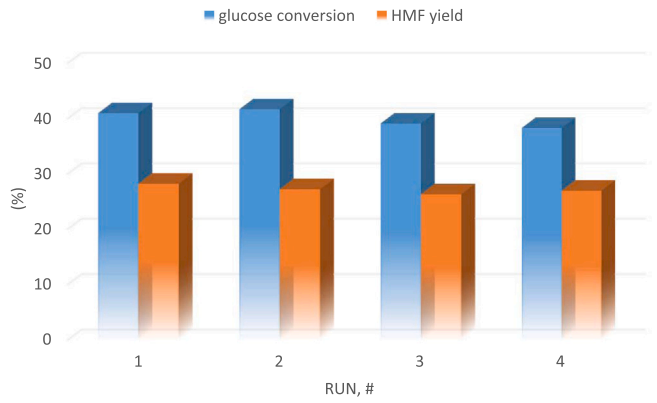

Fig. 7. Recycling study over $CaCl_2$/AC act catalyst (constant glucose/catalyst ratio, T = 180 ºC, time = 12 h, v_{H2O} = 1,5 mL MIBK/H_2O, 7/1, V/V).

4. Conclusions

The impregnation of metal halides on activated charcoal results in a two series of catalysts after different thermal treatment. The later produces a decrease in surface acidity and originates new active sites, such as MOx, confirmed by XRD, especially for the alkali earth chloride series.

The redistribution of the active sites after activation in the bare charcoal affects greatly the catalytic activity. The Bronsted acid sites loss favors the isomerization reaction decreasing the HMF production. The latter is confirmed by the increase in the fructose yield for the AC act in comparison to the AC sample.

For the chloride containing fresh catalysts the HMF yield increases in the $K^+ < Mg^{2+} < Ca^{2+} \approx Sr^{2+}$ order. The better performance of the alkali earth metals is attributed to the formation of glucose – M^{2+} complexes able to immobilize the glucose structure promoting its isomerization. The anion change affects the HMF yield in the $F^- < Cl^- < Br^-$ associated to the increase of the isomerization rate. Hence, no matter the promoting ion, both influences preferentially the glucose to fructose transformation.

The activation and the appearance of diverse active sites affects not only the isomerization reaction but also the dehydration and especially the HMF-glucose (cross)polymerization. In general, for the activated catalysts, higher glucose conversions and minor HMF selectivity are observed in favor to humins production.

Within all series the best catalyst in terms of HMF yield and glucose conversion is $CaCl_2$/AC act sample, due to a great diversity of active sites, such as Bronsted sites (carboxylic groups), basic sites (CaO), and bivalent Lewis acid site (Ca^{2+}). This sample shows also the best dispersion which increases the metal glucose contact.

The reduction of the reaction time provokes glucose conversion and humins selectivity decrease. Again, the $CaCl_2$/AC act sample presents the best activity/selectivity balance. The behavior of the $MgCl_2$/AC act sample does not change with the decrease of the reaction time indicating that the prevailing basic sites for this sample (observed by NH_3-TPD) increase greatly the rate of HMF degradation resulting in humins as main product.

The best performing catalyst is stable and maintains it activity (glucose conversion and selectivity) during four cycles of reutilization.

CRediT authorship contribution statement

Gabriel Delgado Martín: Data curation, Experiment validation, data acquisition and treatment. **Beatriz Lara:** Data acquisition and treatment. **Charf Eddine Bounoukta:** Writing – original draft, data acquisition and treatment. **María Isabel Domínguez:** Methodology, Conceptualization, Project coordination. **Fatima Ammari:** Conceptualization, Supervision. **Svetlana Ivanova:** Catalytic test supervision, Funding acquisition. **Miguel Angel Centeno:** Methodology, Funding acquisition, Project administration, Final manuscript revision.

Declaration of Competing Interest

The authors declare that they have no known competing financial interests or personal relationships that could have appeared to influence the work reported in this paper.

Data availability

Data will be made available on request.

Acknowledgments

Financial support was obtained from Spanish Ministerio de Ciencia e Innovación (MCIN/AEI/10.13039/501100011033/) and for FEDER Funds una manera de hacer Europa), Projects ENE2017-82451-C3-3-R and PID2020-113809RB-C32. Also, the financial support from Junta de Andalucía via Consejería de Transformación Económica, Industria, Conocimiento y Universidades and its PAIDI 2020 program (Grant P18-RT-3405) co-financed by FEDER funds from the European Union are welcomed.

C. Bounoukta acknowledges Universidad de Sevilla and Directorate General for Scientific Research and Technological Development (DGRSTD) of Algerian Ministry of Higher Education (MESRS) for his project scholarship.

Appendix A. Supplementary material

Supplementary data associated with this article can be found in the online version at doi:10.1016/j.cattod.2023.01.019.

References

[1] G. Delgado Martin, C.E. Bounoukta, F. Ammari, M.I. Domínguez, A. Monzón, S. Ivanova, M.Á. Centeno, Fructose dehydration reaction over functionalized nanographitic catalysts in MIBK/H2O biphasic system, Catal. Today 366 (2021) 68–76, https://doi.org/10.1016/j.cattod.2020.03.016.

[2] M. Ohara, A. Takagaki, S. Nishimura, K. Ebitani, Syntheses of 5-hydroxymethylfurfural and levoglucosan by selective dehydration of glucose using solid acid and base catalysts, Appl. Catal. A Gen. 383 (2010) 149–155, https://doi.org/10.1016/j.apcata.2010.05.040.

[3] T. Werpy, G. Petersen. Top Value Added Chemicals from Biomass: Volume I – Results of Screening for Potential Candidates from Sugars and Synthesis Gas, National Renewable Energy Lab, Golden, CO (US), 2004, https://doi.org/10.2172/15008859.

[4] X. Li, Q. Xia, V. Chuc Nguyen, K. Peng, X. Liu, N. Essayem, Y. Wang, High yield production of HMF from carbohydrates over silica–alumina composite catalysts, Catal. Sci. Technol. 6 (2016) 7586–7596, https://doi.org/10.1039/C6CY01628F.

[5] Y. Wang, C.A. Brown, R. Chen, Industrial production, application, microbial biosynthesis and degradation of furanic compound, hydroxymethylfurfural (HMF), AIMS Microbiol 4 (2018) 261–273, https://doi.org/10.3934/microbiol.2018.2.261.

[6] J.K.C.N. Agutaya, R. Inoue, S.S. Vin Tsie, A.T. Quitain, J. de la Peña-García, H. Pérez-Sánchez, M. Sasaki, T. Kida, Metal-free synthesis of HMF from glucose using the supercritical CO_2–subcritical H2O–isopropanol system, Ind. Eng. Chem. Res. 59 (2020) 16527–16538, https://doi.org/10.1021/acs.iecr.0c03551.

[7] I.-J. Kuo, N. Suzuki, Y. Yamauchi, K.C.-W. Wu, Cellulose-to-HMF conversion using crystalline mesoporous titania and zirconia nanocatalysts in ionic liquid systems, RSC Adv. 3 (2013) 2028–2034, https://doi.org/10.1039/C2RA21805D.

[8] L. Zhou, R. Liang, Z. Ma, T. Wu, Y. Wu, Conversion of cellulose to HMF in ionic liquid catalyzed by bifunctional ionic liquids, Bioresour. Technol. 129 (2013) 450–455, https://doi.org/10.1016/j.biortech.2012.11.015.

[9] Y. Su, H.M. Brown, X. Huang, X. Zhou, J.E. Amonette, Z.C. Zhang, Single-step conversion of cellulose to 5-hydroxymethylfurfural (HMF), a versatile platform chemical, Appl. Catal. A Gen. 361 (2009) 117–122, https://doi.org/10.1016/j.apcata.2009.04.002.

[10] B. Kim, J. Jeong, D. Lee, S. Kim, H.-J. Yoon, Y.-S. Lee, J. Ku Cho, Direct transformation of cellulose into 5-hydroxymethyl-2-furfural using a combination of metal chlorides in imidazolium ionic liquid, Green Chem. 13 (2011) 1503–1506, https://doi.org/10.1039/C1GC15152E.

[11] F.C. de Melo, R.F. de Souza, P.L.A. Coutinho, M.O. de Souza, Synthesis of 5-hydroxymethylfurfural from dehydration of fructose and glucose using ionic liquids, J. Braz. Chem. Soc. 25 (2014) 2378–2384, https://doi.org/10.5935/0103-5053.20140256.

[12] A.S. Amarasekara, L.D. Williams, C.C. Ebede, Mechanism of the dehydration of d-fructose to 5-hydroxymethylfurfural in dimethyl sulfoxide at 150°C: an NMR study, Carbohydr. Res. 343 (2008) 3021–3024, https://doi.org/10.1016/j.carres.2008.09.008.
[13] W. Li, T. Zhang, H. Xin, M. Su, L. Ma, H. Jameel, H. Chang, G. Pei, p-Hydroxybenzenesulfonic acid–formaldehyde solid acid resin for the conversion of fructose and glucose to 5-hydroxymethylfurfural, RSC Adv. 7 (2017) 27682–27688, https://doi.org/10.1039/C7RA03155F.
[14] V.V. Ordomsky, V.L. Sushkevich, J.C. Schouten, J. van der Schaaf, T.A. Nijhuis, Glucose dehydration to 5-hydroxymethylfurfural over phosphate catalysts, J. Catal. 300 (2013) 37–46, https://doi.org/10.1016/j.jcat.2012.12.028.
[15] F. Parveen, S. Upadhyayula, Efficient conversion of glucose to HMF using organocatalysts with dual acidic and basic functionalities - a mechanistic and experimental study, Fuel Process. Technol. 162 (2017) 30–36, https://doi.org/10.1016/j.fuproc.2017.03.021.
[16] L. Zhang, G. Xi, Z. Chen, Z. Qi, X. Wang, Enhanced formation of 5-HMF from glucose using a highly selective and stable SAPO-34 catalyst, Chem. Eng. J. 307 (2017) 877–883, https://doi.org/10.1016/j.cej.2016.09.003.
[17] C. Perez Locas, V.A. Yaylayan, Isotope labeling studies on the formation of 5-(hydroxymethyl)-2-furaldehyde (HMF) from sucrose by pyrolysis-GC/MS, J. Agric. Food Chem. 56 (2008) 6717–6723, https://doi.org/10.1021/jf8010245.
[18] I.I. Junior, M.A. do Nascimento, R.O.M.A. de Souza, A. Dufour, R. Wojcieszak, Levoglucosan: a promising platform molecule, Green Chem. 22 (2020) 5859–5880, https://doi.org/10.1039/D0GC01490G.
[19] A. Herbst, C. Janiak, Selective glucose conversion to 5-hydroxymethylfurfural (5-HMF) instead of levulinic acid with MIL-101Cr MOF-derivatives, New J. Chem. 40 (2016) 7958–7967, https://doi.org/10.1039/C6NJ01399F.
[20] G. Tsilomelekis, M.J. Orella, Z. Lin, Z. Cheng, W. Zheng, V. Nikolakis, D.G. Vlachos, Molecular structure, morphology and growth mechanisms and rates of 5-hydroxymethyl furfural (HMF) derived humins, Green Chem. 18 (2016) 1983–1993, https://doi.org/10.1039/C5GC01938A.
[21] A. Ranoux, K. Djanashvili, I.W.C.E. Arends, U. Hanefeld, 5-Hydroxymethylfurfural synthesis from hexoses is autocatalytic, ACS Catal. 3 (2013) 760–763, https://doi.org/10.1021/cs400099a.
[22] C. Antonetti, D. Licursi, S. Fulignati, G. Valentini, A.M. Raspolli Galletti, New frontiers in the catalytic synthesis of levulinic acid: from sugars to raw and waste biomass as starting feedstock, Catalysts 6 (2016) 196, https://doi.org/10.3390/catal6120196.
[23] J. Tang, L. Zhu, X. Fu, J. Dai, X. Guo, C. Hu, Insights into the Kinetics and Reaction Network of Aluminum Chloride-Catalyzed Conversion of Glucose in NaCl–H2O/THF Biphasic System, ACS Publications, 2016, https://doi.org/10.1021/acscatal.6b02515.
[24] Y.J. Pagán-Torres, T. Wang, J.M.R. Gallo, B.H. Shanks, J.A. Dumesic, Production of 5-hydroxymethylfurfural from glucose using a combination of lewis and brønsted acid catalysts in water in a biphasic reactor with an alkylphenol solvent, ACS Catal. 2 (2012) 930–934, https://doi.org/10.1021/cs300192z.
[25] G. Tsilomelekis, T.R. Josephson, V. Nikolakis, S. Caratzoulas, Origin of 5-hydroxymethylfurfural stability in water/dimethyl sulfoxide mixtures, ChemSusChem 7 (2014) 117–126, https://doi.org/10.1002/cssc.201300786.
[26] V. Vasudevan, S.H. Mushrif, Insights into the solvation of glucose in water, dimethyl sulfoxide (DMSO), tetrahydrofuran (THF) and N,N-dimethylformamide (DMF) and its possible implications on the conversion of glucose to platform chemicals, RSC Adv. 5 (2015) 20756–20763, https://doi.org/10.1039/C4RA15123B.
[27] Z. Wei, J. Lou, Z. Li, Y. Liu, One-pot production of 2,5-dimethylfuran from fructose over Ru/C and a Lewis–Brønsted acid mixture in N, N -dimethylformamide, Catal. Sci. Technol. 6 (2016) 6217–6225, https://doi.org/10.1039/C6CY00275G.
[28] K. Beckerle, J. Okuda, Conversion of glucose and cellobiose into 5-hydroxymethylfurfural (HMF) by rare earth metal salts in N,N′-dimethylacetamide (DMA), J. Mol. Catal. A Chem. 356 (2012) 158–164, https://doi.org/10.1016/j.molcata.2012.01.008.
[29] Q. Ren, Y. Huang, H. Ma, F. Wang, J. Gao, J. Xu, Conversion of glucose to 5-hydroxymethylfurfural catalyzed by metal Halide in N,N-dimethylacetamide, BioResources 8 (2013) 1563–1572.
[30] Molecular aspects of glucose dehydration by chromium chlorides in ionic liquids - Zhang - 2011 - Chem. Eur. J., Wiley Online Library, (n.d.). ⟨https://chemistry-europe.onlinelibrary.wiley.com/doi/full/10.1002/chem.201003645?casa_token=CPocjB1-gtMAAAAA%3AqqJPMcnwagP485G8Bf_FC5NbNcOvsf6oW7lv8Eq9gLyY81TEDyM8G1JXdC4bMv_Uyf76vLzyXGix2w⟩, (Accessed 21 June 2022).
[31] X. Qi, M. Watanabe, T.M. Aida, R.L. Smith, Synergistic conversion of glucose into 5-hydroxymethylfurfural in ionic liquid–water mixtures, Bioresour. Technol. 109 (2012) 224–228, https://doi.org/10.1016/j.biortech.2012.01.034.
[32] Q. Hou, M. Zhen, L. Liu, Y. Chen, F. Huang, S. Zhang, W. Li, M. Ju, Tin phosphate as a heterogeneous catalyst for efficient dehydration of glucose into 5-hydroxymethylfurfural in ionic liquid, Appl. Catal. B Environ. 224 (2018) 183–193, https://doi.org/10.1016/j.apcatb.2017.09.049.
[33] Y. Qu, C. Huang, Y. Song, J. Zhang, B. Chen, Efficient dehydration of glucose to 5-hydroxymethylfurfural catalyzed by the ionic liquid,1-hydroxyethyl-3-methylimidazolium tetrafluoroborate, Bioresour. Technol. 121 (2012) 462–466, https://doi.org/10.1016/j.biortech.2012.06.081.
[34] X. Qi, M. Watanabe, T.M. Aida, J. Richard Lee Smith, Catalytic dehydration of fructose into 5-hydroxymethylfurfural by ion-exchange resin in mixed-aqueous system by microwave heating, Green Chem. 10 (2008) 799–805, https://doi.org/10.1039/B801641K.
[35] T. Zhang, W. Li, H. Xin, L. Jin, Q. Liu, Production of HMF from glucose using an Al3+-promoted acidic phenol-formaldehyde resin catalyst, Catal. Commun. 124 (2019) 56–61, https://doi.org/10.1016/j.catcom.2019.03.001.
[36] K. Li, M. Du, P. Ji, Multifunctional tin-based heterogeneous catalyst for catalytic conversion of glucose to 5-hydroxymethylfurfural, ACS Sustain. Chem. Eng. 6 (2018) 5636–5644, https://doi.org/10.1021/acssuschemeng.8b00745.
[37] J. Wang, W. Xu, J. Ren, X. Liu, G. Lu, Y. Wang, Efficient catalytic conversion of fructose into hydroxymethylfurfural by a novel carbon-based solid acid, Green Chem. 13 (2011) 2678–2681, https://doi.org/10.1039/C1GC15306D.
[38] N.V. Gromov, T.B. Medvedeva, O.P. Taran, A.V. Bukhtiyarov, C. Aymonier, I. P. Prosvirin, V.N. Parmon, Hydrothermal solubilization–hydrolysis–dehydration of cellulose to glucose and 5-hydroxymethylfurfural over solid acid carbon catalysts, Top. Catal. 61 (2018) 1912–1927, https://doi.org/10.1007/s11244-018-1049-4.
[39] M. Shaikh, A. Sahu, A.K. Kumar, M. Sahu, S.K. Singh, K.V.S. Ranganath, Metal-free carbon as a catalyst for oxidative coupling: solvent-enhanced poly-coupling with regioselectivity, Green Chem. 19 (2017) 4533–4537, https://doi.org/10.1039/C7GC02227A.
[40] P. Wrigstedt, J. Keskiväli, M. Leskelä, T. Repo, The role of salts and Brønsted acids in Lewis acid-catalyzed aqueous-phase glucose dehydration to 5-hydroxymethylfurfural, ChemCatChem 7 (2015) 501–507, https://doi.org/10.1002/cctc.201402941.
[41] J.L. Santos, L.F. Bobadilla, M.A. Centeno, J.A. Odriozola, Operando DRIFTS-MS study of WGS and rWGS reaction on biochar-based Pt catalysts: the promotional effect of Na, C 4 (2018) 47, https://doi.org/10.3390/c4030047.
[42] J.L. Santos, P. Mäki-Arvela, A. Monzón, D.Y. Murzin, M.Á. Centeno, Metal catalysts supported on biochars: Part I synthesis and characterization, Appl. Catal. B Environ. 268 (2020), 118423, https://doi.org/10.1016/j.apcatb.2019.118423.
[43] C. Fan, H. Guan, H. Zhang, J. Wang, S. Wang, X. Wang, Conversion of fructose and glucose into 5-hydroxymethylfurfural catalyzed by a solid heteropolyacid salt, Biomass Bioenergy 35 (2011) 2659–2665, https://doi.org/10.1016/j.biombioe.2011.03.004.
[44] J. Collins, D. Zheng, T. Ngo, D. Qu, M. Foster, Partial graphitization of activated carbon by surface acidification, Carbon 79 (2014) 500–517, https://doi.org/10.1016/j.carbon.2014.08.009.
[45] M.M. Rahman, M. Muttakin, A. Pal, A.Z. Shafiullah, B.B. Saha, A statistical approach to determine optimal models for IUPAC-classified adsorption isotherms, Energies 12 (2019) 4565, https://doi.org/10.3390/en12234565.
[46] G. Leofanti, M. Padovan, G. Tozzola, B. Venturelli, Surface area and pore texture of catalysts, Catal. Today 41 (1998) 207–219, https://doi.org/10.1016/S0920-5861(98)00050-9.
[47] A.K. Galwey, G.M. Laverty, The thermal decomposition of magnesium chloride dihydrate, Thermochim. Acta 138 (1989) 115–127, https://doi.org/10.1016/0040-6031(89)87246-6.
[48] Q. Huang, G. Lu, J. Wang, J. Yu, Thermal decomposition mechanisms of MgCl2·6H2O and MgCl2·H2O, J. Anal. Appl. Pyrolysis 91 (2011) 159–164, https://doi.org/10.1016/j.jaap.2011.02.005.
[49] S.A. Chernyak, A.S. Ivanov, K.I. Maslakov, A.V. Egorov, Z. Shen, S.S. Savilov, V. V. Lunin, Oxidation, defunctionalization and catalyst life cycle of carbon nanotubes: a Raman spectroscopy view, Phys. Chem. Chem. Phys. 19 (2017) 2276–2285, https://doi.org/10.1039/C6CP04657F.
[50] Y. Kouketsu, T. Mizukami, H. Mori, S. Endo, M. Aoya, H. Hara, D. Nakamura, S. Wallis, A new approach to develop the Raman carbonaceous material geothermometer for low-grade metamorphism using peak width, Isl. Arc 23 (2014) 33–50, https://doi.org/10.1111/iar.12057.
[51] H. Ge, Z. Ye, R. He, Raman spectroscopy of diesel and gasoline engine-out soot using different laser power, J. Environ. Sci. 79 (2019) 74–80, https://doi.org/10.1016/j.jes.2018.11.001.
[52] N. Rodríguez, Y.Y. Agámez-Pertuz, E. Romero, J. de, J. Díaz-Velásquez, J. A. Odriozola, M.Á. Centeno, Effect of starch as binder in carbon aerogel and carbon xerogel preparation, J. Non-Cryst. Solids 522 (2019), 119554, https://doi.org/10.1016/j.jnoncrysol.2019.119554.
[53] M. Nabil, K.R. Mahmoud, A. El-Shaer, H.A. Nayber, Preparation of crystalline silica (quartz, cristobalite, and tridymite) and amorphous silica powder (one step), J. Phys. Chem. Solids 121 (2018) 22–26, https://doi.org/10.1016/j.jpcs.2018.05.001.
[54] P. Stacey, K.T. Mader, C. Sammon, Feasibility of the quantification of respirable crystalline silica by mass on aerosol sampling filters using Raman microscopy, J. Raman Spectrosc. 48 (2017) 720–725, https://doi.org/10.1002/jrs.5113.
[55] A. Černok, K. Marquardt, R. Caracas, E. Bykova, G. Habler, H.-P. Liermann, M. Hanfland, M. Mezouar, E. Bobocioiu, L. Dubrovinsky, Compressional pathways of α-cristobalite, structure of cristobalite X-I, and towards the understanding of seifertite formation, Nat. Commun. 8 (2017) 15647, https://doi.org/10.1038/ncomms15647.
[56] X. Li, K. Peng, X. Liu, Q. Xia, Y. Wang, Comprehensive understanding of the role of brønsted and lewis acid sites in glucose conversion into 5-hydromethylfurfural, ChemCatChem 9 (2017) 2739–2746, https://doi.org/10.1002/cctc.201601203.
[57] P. Drabo, M. Fischer, V. Toussaint, F. Flecken, R. Palkovits, I. Delidovich, What are the catalytically active species for aqueous-phase isomerization of D-glucose into

D-fructose in the presence of alkaline earth metal (hydr)oxides? J. Catal. 402 (2021) 315–324, https://doi.org/10.1016/j.jcat.2021.08.036.

[58] C. García-Sancho, I. Fúnez-Núñez, R. Moreno-Tost, J. Santamaría-González, E. Pérez-Inestrosa, J.L.G. Fierro, P. Maireles-Torres, Beneficial effects of calcium chloride on glucose dehydration to 5-hydroxymethylfurfural in the presence of alumina as catalyst, Appl. Catal. B Environ. 206 (2017) 617–625, https://doi.org/10.1016/j.apcatb.2017.01.065.

[59] X. Hu, C.-Z. Li, Levulinic esters from the acid-catalysed reactions of sugars and alcohols as part of a bio-refinery, Green Chem. 13 (2011) 1676–1679, https://doi.org/10.1039/C1GC15272F.